

Programmable Digital Weaves

Yue Li¹ Juan Montes¹ Bernhard Thomaszewski¹ Stelian Coros¹

Abstract—Elastic lattice-like materials whose structures can be tuned to achieve desired mechanical properties hold great promise for many applications in robotics. However, existing methods rely on all-fused connections at lattice nodes, which limits the range of mechanical properties that can be achieved. In this work, we introduce Programmable Digital Weaves—3D-printable, textile-like materials with sliding connections that mimic the yarn structure of conventional woven fabrics. Our method allows for relative motion between crossing strands, thus unlocking a large space of programmable nonlinear and anisotropic material behavior. As we demonstrate through a set of virtual and physical experiments, this new concept extends to a wide variety of patterns, ranging from regular arrangements of orthogonal strands similar to conventional woven fabrics to curved yarns, interlacing closed loops, and dedicated strands for actuation.

Index Terms—Robotics material, metamaterial, computational design, additive manufacturing, Eulerian-on-Lagrangian simulation, homogenization.

I. INTRODUCTION

STRUCTURED sheet materials with programmable mechanical properties have many applications in soft robotics, wearable haptics, and medical devices [1]. These sheets are typically implemented as planar networks of elastic beams whose parameters—edge shape and orientation, network density and connectivity—can be controlled to create materials with tailored stiffness profiles [2]. While these custom materials can readily be manufactured using laser cutting or 3D printing, existing methods rely on all-fused connections, which prohibits relative motion between incident beams and, consequently, limits the range of deformation and mechanical properties that can be achieved.

In this work, we extend the concept of structured sheet materials to programmable digital weaves (PDWs): 3D-printable, textile-like materials with sliding connections that mimic the yarn structure of conventional woven fabrics. The internal degrees of freedom of programmable digital weaves allow for extreme contrast in directional tensile stiffness, and we show that a broad range of mechanical behavior—from highly anisotropic to quasi-isotropic—can be obtained through strategic assignment of fused and slip connections.

Manuscript received: September 9, 2021; Revised: December 3, 2021; Accepted: January 6, 2022.

This paper was recommended for publication by Editor Kyu-Jin Cho upon evaluation of the Associate Editor and Reviewers' comments.

This research was supported by the European Research Council (ERC) under the European Union's Horizon 2020 research and innovation program (Grant No. 866480) and the Swiss National Science Foundation (Grant No. 200021_200644).

¹ The authors are with the Computer Science Department, ETH Zurich, Switzerland {yue.li, jmontes, bthomasz, scoros}@inf.ethz.ch.

Digital Object Identifier (DOI): see top of this page.

On a technical level, we implement sliding connections using small-scale channels that allow for relative tangential motion between crossing strands while preventing separation; see Fig. 2. This approach lends itself to a one-shot fully-automated fabrication process that only requires a consumer-level fused filament 3D printer, which is controlled through custom G-code instructions.

As we show through our experiments, this methodology allows for a wide variety of patterns, ranging from regular arrangements of orthogonal strands similar to conventional woven fabrics to curved yarns, interlacing closed loops, and dedicated fibers for actuation. To predict the performance of such complex weaves before manufacturing, we further propose a dedicated computational model based on an existing yarn-level simulation code.

To explore the design space offered by programmable digital weaves, we perform simulation experiments for various pattern and connection parameters. We quantitatively analyse the impact of these design parameters on macromechanical performance using simulation-based homogenization. To test the feasibility of our designs, we fabricate a set of 3D-printed prototypes and observe good agreement between our simulation results and real-world behavior.

II. RELATED WORK

The design of materials with tailored mechanical properties is of great importance in the field of soft robotics. For example, custom materials can give robots increased flexibility, strength and protection, as well as enabling safer interaction with humans.

Mechanical Metamaterials: Mechanical metamaterials achieve desired macro-mechanical properties by virtue of architected micro- or meso-structure. For conciseness, we only discuss work on planar metamaterials—or metasheets—and refer to Bertoldi *et al.* [3] for an extensive review of flexible mechanical metamaterials. Focusing on isohedral tilings, a particular class of patterns, Schumacher *et al.* [2] characterized the macro-mechanical behaviour of 3D-printed structured sheets using data-driven homogenization. To generate metasheets with locally varying material properties, Martinez *et al.* [4] introduce generalized Voronoi tilings based on star-shaped metrics that allow for continuous transitions between different patterns. With a similar goal in mind, Djourachkovich *et al.* [5] address the problem of decoupling cell geometry from mechanical properties. In comparison to our channeled connections, these structures are more limited in the range of deformation they can achieve for the same applied force.

3D-Printed Weaves: Whereas 3D-printed mechanical metasheets have been studied intensively, only few works have

attempted to emulate the yarn structure of woven fabrics. Takahashi and Kim [6] describe a process for creating digital textiles by routing 3D-printed thread through a jig, i.e., a set of vertical pillars. The resulting undulation in the strands leads to stretchable sheet materials with controllable thickness and interesting visual properties. Compared to our planar fabrication process, however, their vertical weaving approach limits flexibility in terms of yarn shapes and layouts. Similar in spirit, Forman *et al.* [7] exploit an under-extrusion artifact of fused filament fabrication printers to create thin, tulle-like sheets with high flexibility and structural detail. However, whereas their sheets derive macro-mechanical compliance from elastic deformations at the native scale, our digital weaves achieve flexibility through internal yarn sliding.

Robotic Materials: Generalizing materials with tailored mechanical properties, robotic materials extend passive substrates with actuation, sensing and communication structures [8]. In the direction of extending fabrics, Buckner *et al.* [9] augmented passive textiles with active fibers for sensing and actuation to achieve desired locomotion targets. Using shape memory fibers, Chenal *et al.* [10] proposed a stability brace for human finger joints that allows for variable stiffness. Hiramitsu *et al.* [11] developed an active textile-like garment by knitting artificial muscles in the warp direction with strings in the weft direction. Shi *et al.* [12] explore the fabrication and integration of microelectronic systems into textile fabrics. Whereas most research on robotic materials has so far followed the dichotomy of *passive* substrates and *active* secondary structure, Sanchez *et al.* [13] advocate an *active programmable textile* paradigm which puts fabric, actuation, and sensing structures on an equal footing. Our approach follows this line of thought by integrating active and passive strands in a fully automated fabrication process.

Modeling Weaves: Physics-based modeling of elastic rods is a problem that has received much attention from the graphics community [14], [15]. Originally developed for the purpose of computer animation, the discrete elastic rod model by Bergou *et al.* [16] has been used for a variety of real-world applications, including robotic wire cutting [17], elastic grid-shells *et al.* [18] and structured sheet materials [2]. This model has also been extended to incorporate the physical behaviour of fused rod connections [19], connections with free rotations [20], and sliding between yarns in woven cloth [21]. Our computational model builds on the work by Cirio *et al.* [21], with extensions that allow sliding connections on initially curved yarns. Complementing these native-scale simulation models, Schumacher *et al.* [2] and Sperl *et al.* [22] developed homogenized, macro-mechanical descriptions and material models, respectively. We draw on these ideas to analyze the macro-mechanical behavior of our programmable digital weaves in a quantitative way.

III. DIGITAL WEAVES

Our approach for programmable digital weaves (PDWs) is based on a simple idea: we augment planar elastic grids, in which all crossings between strands are fused, with sliding connections that allow for relative tangential motion between

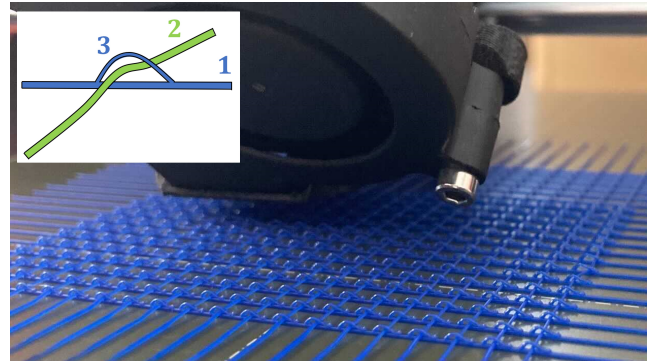


Fig. 1. A snapshot of the 3D printing process for a regular digital weave with all-sliding connections. All channels have the same orientation, leaving the orthogonal direction free for sliding motions. With 20×20 strands on an $8\text{cm} \times 8\text{cm}$ patch, the printing process takes about 40 minutes. The printing sequence is shown in the top-left corner.

strands. We start the technical description of our method with its practical implementation and corresponding manufacturing process. We then describe our computational model for PDWs that serves as a basis for virtual prototyping and design exploration. Finally, we briefly summarize how to compute macro-mechanical descriptions of programmable digital weaves.

A. Manufacturing

To create sliding connections in practice, we proceed in three steps. We first print one of the crossing strands in the usual way, i.e., by following a planar path. The second strand is printed by lifting the print head slightly before crossing the bottom-layer strand. Using appropriate settings for velocity, extrusion rate, and nozzle temperature, this motion leads to well separated strands with little or no adhesion. Finally, we print an arc-shaped channel that is fused to the bottom-layer strand, enclosing the crossing strand without connecting to it. A snapshot of the printing process can be seen in Fig 1. We implement the above strategy using custom G-code that can be run on any conventional 3D printer based on fused filament fabrication. We use a Prusa I3 MK3¹ with PLA filament for all prototypes and results reported in this work. The nozzle temperature is set to 180 and we pre-heat the print bed to 60 degrees. We set the extrusion rate based on the nozzle diameter (0.4mm), filament radius (1.75mm), desired strand width (0.5mm) and print head velocity. The latter is set to 600 mm/min by default and 300 mm/min when printing channels. Arc-shaped channels are created by moving the print head along a triangle path with the bottom edge centered at the crossing node. For better print quality, we decrease velocity when printing channels. We furthermore extend the second half of the channel by 20% compared to the length of the first half in order to avoid spurious connections with the sliding strand due to sagging. The channel height is set to twice the strand width (1.0mm).

¹<https://www.prusa3d.com/original-prusa-i3-mk3/>

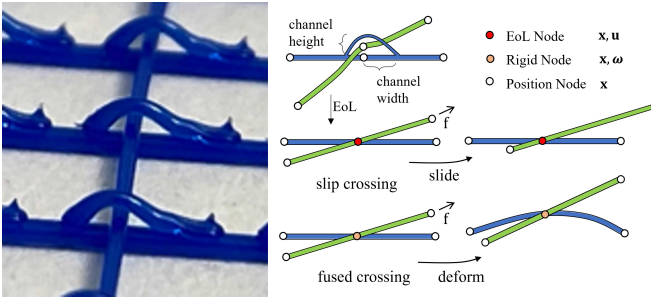


Fig. 2. Close-up of 3D-printed channels at sliding connections (*left*) and schematic view of the corresponding simulation model (*middle*). To represent crossing strands in persistent contact, Our Eulerian-on-Lagrangian (EoL) discretization uses a single node \mathbf{x} augmented by Eulerian DoFs \mathbf{u} to model sliding. Fused crossings are modeled as rigid bodies with additional rotational DoFs $\boldsymbol{\omega}$. The right column shows an example with an axial force applied along the green strand. The sliding connection leads to simple translation of the green strand, whereas the fused connection induces planar bending deformations in the blue strand.

B. Simulation

Programmable Digital Weaves can exhibit complex mechanical behavior characterized by strong nonlinearity and anisotropy. Predicting the performance of a given weave, or design, can be difficult and time consuming when relying solely on intuition. To allow for virtual prototyping of digital weaves and rapid design exploration, we propose a dedicated computational model that extends existing work for yarn-level cloth simulation [21], [15] to support sliding connections on initially curved yarns. As can be seen from our physical prototypes (Fig.2), the geometry of the channels restricts the movement of the strands, leading to persistent contacts. Based on this intrinsic property of our PDWs, we build on the Eulerian-On-Lagrangian (EoL) approach from Cirio *et al.* [21]. More concretely, we model each location where strands come into contact as a single nodal point $\mathbf{x}_i \in \mathbb{R}^3$, where sliding between crossing strands is achieved by introducing one Eulerian DoF $u_i^j \in \mathbb{R}$ for each strand j crossing a contact point i . Since persistent contacts are built into the discretization, we avoid the need for computationally-expensive contact detection and handling.

Our models are printed as a 2D rod network with (potentially) curved strands. However, the original EoL implementation by Cirio *et al.* [21] assumes *naturally straight* rods, where the Eulerian DoFs are parameterized by arc-length. For our purpose, we extend this approach to *naturally curved* rods by modeling their rest configurations as a collection of C^2 -continuous, planar, interpolating splines [23]. These splines offer a smooth representation for the Eulerian DoFs, allowing the use of efficient continuous optimization methods for simulation. Whereas under the sliding yarns model the undeformed configuration was fully contained in 1D, our solution maps Eulerian DoFs in 1D to points in 2D through the parameterization $\mathbf{X}(u_i) : \mathbb{R} \rightarrow \mathbb{R}^2$, allowing the use of naturally curved rods. Rods can stretch, bend and twist. While stretch is trivial to compute from our current discretization, modeling bending and twisting deformations requires additional information. To this end, we add a rotational DoF θ_i for each two consecutive rod nodes $\{\mathbf{x}_i, \mathbf{x}_{i+1}\}$, representing the twist of an adapted

frame with respect to the center-line of the edge connecting the two nodes. Bending and twisting deformation between edges can then be computed from the relative rotations between two adapted frames [16]. The bending and twisting behavior at crossing points requires extra care for our application. While sliding strands can freely rotate and twist with respect to each other, strands crossing in fused connections exhibit stiffer behavior. Following Zehnder *et al.* [19], we restrain the relative motion of the strands crossing in a fused connection \mathbf{x}_k with additional rotational DoFs $\boldsymbol{\omega}_k \in \mathbb{R}^3$. These rotational DoFs provide a common rigid frame of reference shared by the fused strands with the objective of capturing their bending and twisting deformation relative to each other. For our stretching, bending and twisting energies, we adopt the discrete energy model of Bergou *et al.* [16]. This model has been thoroughly studied and its predictive power confirmed in the context of various applications. As we show through our examples, We likewise obtained excellent agreement between simulation results and physical prototypes.

The rod network is then governed by the following potential energy,

$$\begin{aligned} E_{\text{rods}}(\mathbf{x}, \mathbf{X}(\mathbf{u}), \mathbf{u}, \boldsymbol{\theta}, \boldsymbol{\omega}) = & E_{\text{stretch}}(\mathbf{x}, \mathbf{X}(\mathbf{u})) \\ & + E_{\text{bend}}(\mathbf{x}, \mathbf{X}(\mathbf{u}), \boldsymbol{\theta}) \\ & + E_{\text{twist}}(\mathbf{x}, \mathbf{X}(\mathbf{u}), \boldsymbol{\theta}) + E_{\text{rigid}}(\mathbf{x}, \boldsymbol{\omega}) \\ & + E_{\text{contact}}(\mathbf{u}) + E_{\text{reg}}(\mathbf{u}), \end{aligned}$$

where $\mathbf{x}, \mathbf{X}(\mathbf{u})$ denotes the deformed and undeformed nodal positions, \mathbf{u} are the Eulerian DoFs, $\boldsymbol{\omega}$ are the Euler angles for the rotational DoFs of the fused crossings, and $\boldsymbol{\theta}$ represent the twists of the adapted frames. The E_{contact} term enforces a minimal distance between two crossings [21] and E_{reg} is a small penalty term on the l^2 -norm of the Eulerian variables emulating a small frictional force. We refer to the original papers for the definition of each individual term. Computing equilibrium configurations for our weaves amounts to solving the following optimization problem,

$$\min_{\mathbf{q}} E_{\text{rod}}(\mathbf{q}) \quad \text{s.t.} \quad \mathbf{D}\mathbf{q} = \mathbf{q}^*, \quad (1)$$

where \mathbf{q} stacks all of our system DoFs $(\mathbf{x}, \mathbf{u}, \boldsymbol{\omega}, \boldsymbol{\theta})$ in to a vector, \mathbf{q}^* denotes the target prescription, and the matrix \mathbf{D} imposes Dirichlet boundary conditions via variable substitution. We solve this unconstrained minimization problem using Newton's method with line search and dynamic regularization. To obtain a sparse Hessian, at each Newton iteration we perform time parallel transport [16], and accumulate rotation angles [19] to avoid singular configurations.

C. Homogenization

To characterize the macro-mechanical behavior of our digital weaves in a concise way, we resort to a numerical homogenization method that leverages simulation data from virtual tensile tests [2]. Concretely, we perform simulations on tileable unit cells subjected to uniaxial strain in a given direction \mathbf{d} and periodic boundary conditions, which are enforced via penalty terms. For each of these virtual tensile test, we compute the

corresponding directional Young's modulus E and Poisson ratio ν as

$$E = \frac{\mathbf{d}^T \boldsymbol{\sigma}_{\text{macro}} \mathbf{d}}{\mathbf{d}^T \boldsymbol{\epsilon}_{\text{macro}} \mathbf{d}}, \quad \nu = \frac{\mathbf{n}^T \boldsymbol{\epsilon}_{\text{macro}} \mathbf{n}}{\mathbf{d}^T \boldsymbol{\epsilon}_{\text{macro}} \mathbf{d}} \quad (2)$$

where \mathbf{n} is orthogonal to \mathbf{d} and $\boldsymbol{\sigma}_{\text{macro}}, \boldsymbol{\epsilon}_{\text{macro}}$ are the homogenized stress and strain computed from the boundary of the unit cell [2]. For all homogenization results shown in this work, we sample uniaxial strain directions ranging from 0 to 180 degrees at 200 uniformly distributed locations.

IV. RESULTS

In this section, we explore the possibilities enabled by our programmable digital weaves. Starting with a regular weave, we then explore interlacing structures with straight and curved loops. For each case, we show that, by combining different choices for fused and sliding connections, we obtain vast range of nonlinear mechanical behavior ranging from quasi-isotropic to highly anisotropic. Finally we demonstrate a planar-to-parabolic deployment example, indicating the potential of our approach for integration of embedded actuation systems.

A. Design Explorations on Conventional Weave Patterns

We first examine the qualitative changes in mechanical behavior induced by introducing sliding connections to a regular weave with all-fused connections. As can be seen from Fig. 3, when subjected to shearing forces applied diagonally to the principal strand directions, the structure with fused connections deforms out of plane in order to reduce the stretching energy. When replacing fused with sliding connections, however, we instead observe large planar deformations characterized by rotation and sliding motion at strand crossings. Both scenarios are well predicted by our simulation model. Strain in the direction of strands leads to the same stiffness

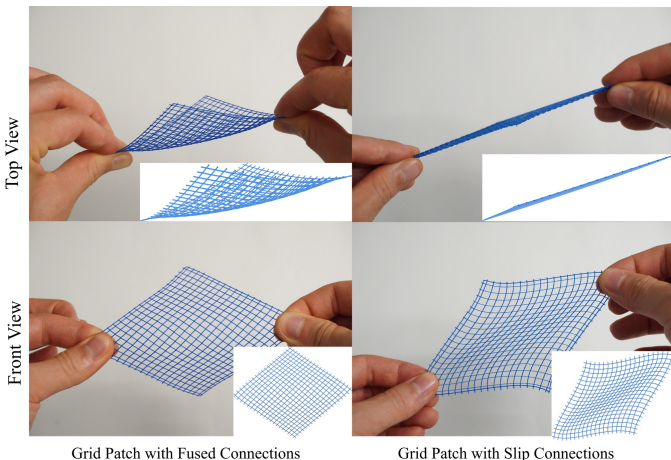


Fig. 3. Qualitative comparisons of simulation results and corresponding physical counterparts. As can be seen from these images, the simulation model provides good predictive capacity for both types of connections, i.e., out-of-plane bending (all-fused connections, left) and in-plane shearing (all-slip connections, right).

response regardless of the choice of fused/slip connections. This is due to the fact that strands on the orthogonal direction

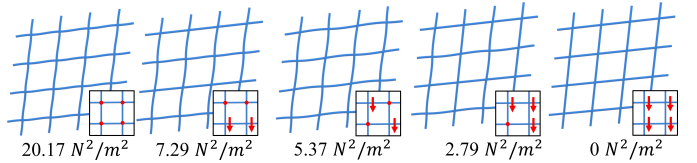


Fig. 4. Shear stiffness response of a regular weave pattern with different combinations of fused-slip connections. Simulation results with corresponding fused-slip assignments shown at the bottom-right corner of each structure, with red circles indicating fused connections and red arrows indicating sliding directions, respectively. The stiffness for diagonal loading is listed at the bottom of each structure.

to the imposed strain exhibit no deformation at all. However, when shearing stress is applied, slip connections can freely rotate among themselves whereas fused connections resist the imposed force through bending. As can be observed from these experiments, exploring the combinatorial space of a 2×2 unit cell can already lead to structures with very different mechanical responses. The simulation results and the directional stiffness values at 45 degrees can be seen in Fig. 4.

B. Meta-Material Designs with Interlacing Loops

Our method generalizes beyond regular lattices structures and can be applied to curved rods and interlacing loops. In the first example, we examine the impact of fused and sliding connections on samples made from interlaced squares. At each corner where two squares intersect, the two crossings can either be all-fused or have a channel in one of the two directions of the square. We design and fabricate four

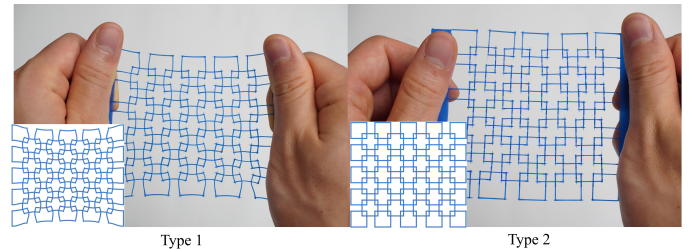


Fig. 5. Qualitative comparison of simulation results and corresponding physical counterparts for the interlacing squares example. Left: all-fused connections. Right: connections enabling free sliding in the horizontal direction. Note that for the structure on the right, all imposed deformation is absorbed by internal sliding, leading to zero stiffness in the horizontal direction.

structures corresponding to representative examples of a high-dimensional design space. The two structures exhibiting the most prominent difference in stretching along the horizontal direction of the image plane are shown in Fig. 5. As a first experiment, we impose a uniaxial strain of 10% for all combinations and compute their directional Young's moduli and Poisson's ratios (Fig 6). When using all-fused connections (Type 1), the material responses appear to be quasi-isotropic and are relatively stiff in all directions. When substituting all fused connections with channels that allow sliding in the horizontal direction of the image plane (Type 2), we observe a significant change in the stiffness profile, with zero stiffness in the horizontal direction. This is explained by the fact that the imposed deformation is entirely absorbed by internal sliding.

We then change the direction of one out of two channels to allow for vertical sliding motion (Type 3). The corresponding structure exhibits an orthotropic material response. For the last example, we fuse two crossings (at the bottom-left corner of the unit cell) for the Type 3 pattern, which leads to a highly anisotropic material response (Type 4). Since the homogenization plots indicate major difference for these four structures at 45 degrees, we further study the non-linear deformation space by imposing the same force in this direction to all structures. Fig. 6 shows significantly larger deformations for structure Type 1 and 2, indicating a lower stiffness. The same force, however, leads to visually imperceptible deformation for those involving fused connections or, equivalently, higher stiffness. We refer to the supplemental video for manipulation sequences of the printed structures.

In the second experiment, we select the Type 2 structure and conduct homogenization with small and large strains. As

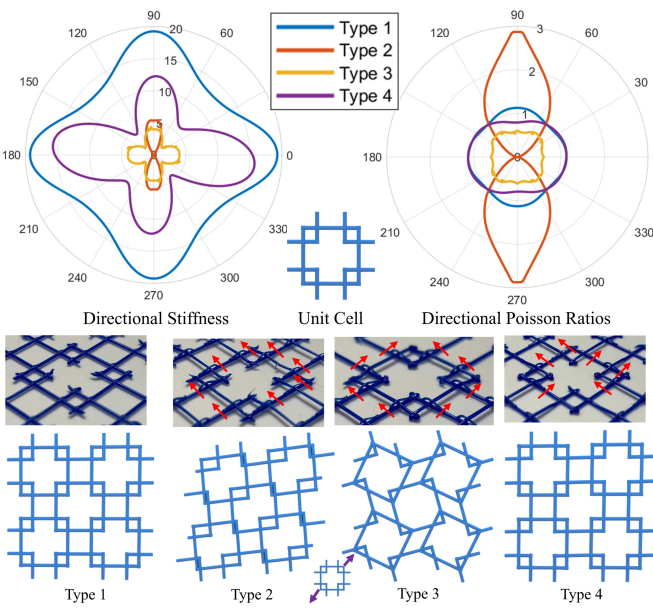


Fig. 6. Interlacing squares. The different fused-slip connections for the four structures considered are shown on the physical prototypes with sliding directions indicated with red arrows (middle row). As shown in the stiffness profiles (top row), these structures exhibit widely different mechanical behaviors, ranging from quasi-isotropic (Type 1) to highly anisotropic (Type 4). Simulation results of these structures (bottom row) are obtained for the same applied load (diagonal direction indicated with purple arrows). It can be seen that the sliding mechanisms of the Type 2 and 3 structures are fully triggered while the ones involving fused connections remains largely undeformed.

can be seen from Fig. 7, until the squares reach their sliding limits, the structure exhibits zero stiffness. However once the imposed strain is larger than the absorption limit of the internal sliding mechanism, finite stiffness is observed. We visualize the simulation results at selected strain directions to further demonstrate that predicting the nonlinear deformation behavior solely on intuition is extremely challenging.

Programmable digital weaves can be readily applied to curved geometries. In the example shown in Fig. 8, we replace the squares in the previous example with circles. Each circle overlaps with its four neighbors by 10% of its radius (0.8 cm), leading to eight crossing points per circle. We explore the two

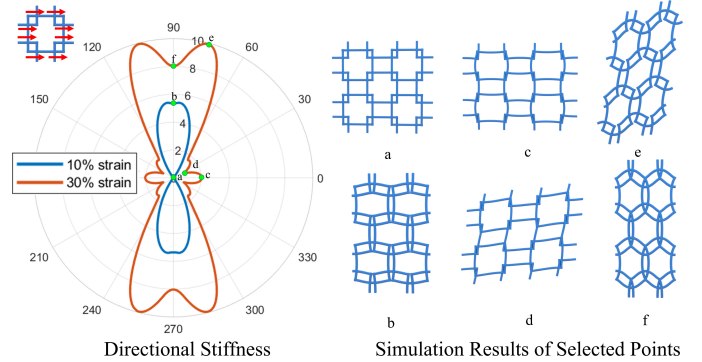


Fig. 7. Nonlinear mechanical behavior. Here we show the deformations of our Type 2 structure when imposing uni-axial strain of 10 and 30 percent, respectively. The zero stiffness response shown initially by this structure for small imposed strains is in sharp contrast to the response for larger strains, indicating highly nonlinear behavior. The sliding directions of the channels on the unit cell is shown in the top-left corner.

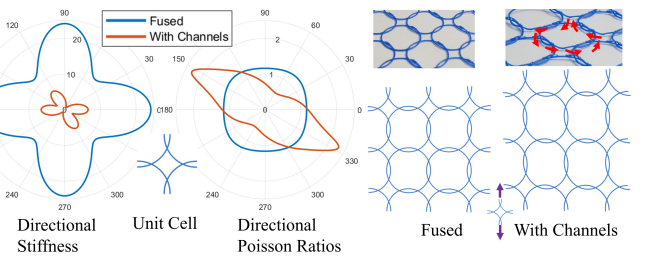


Fig. 8. Interlacing circles. We explore the option of curved strands using circular loops. As indicated by the plots for directional stiffness and Poisson ratios, replacing all-fused with all-slip connections significantly modifies the mechanical properties. Due to the asymmetric orientation of the channels, the mechanical response is thus asymmetric along the diagonal direction. As an example, we show the simulation results for both structures induced by the same force along the vertical direction of the image plane (purple arrows). The sliding directions at the crossings are shown with red arrows.

extreme options of all-fused and all-sliding connections for these eight crossing points. Fig. 8 indicates that the all-fused variant results in an orthotropic stiffness response while its all-sliding counterpart leads to a highly anisotropic behavior. On the right of this figure, compare the resulting deformations for the same imposed for (along the vertical direction of the image plane). Qualitatively, it can be noted that the individual circles of the all-sliding structure have been distorted into ellipses, whereas the ones with the fused connections remain largely circular.

C. Actuation

Leveraging the possibility to combine fused and slip connections in a single design, we further explore how strands can be used to implement embedded actuation. In this example, we design a structure with the goal of achieving a planar-to-parabolic deployment motion by virtue of a single actuation strand. As can be seen from Fig. 9, the tip of the vertical actuation strand is fused to the outer circle but can freely slide on all the other crossings (red arrows). All other connections are fused. We impose sufficient boundary conditions by fixing the position of the bottom-most crossing of the actuation strand and the outer ring. Actuation is achieved by applying a compressive axial force at the bottom of the actuation strand.

As can be seen in Fig. 9, our simulation again shows good agreement with the physical experiment. We emphasize that manufacturing of these actuation strands is fully automatic without any manual assembly required. We refer to the supplemental video for a real-world actuation sequence for this design.

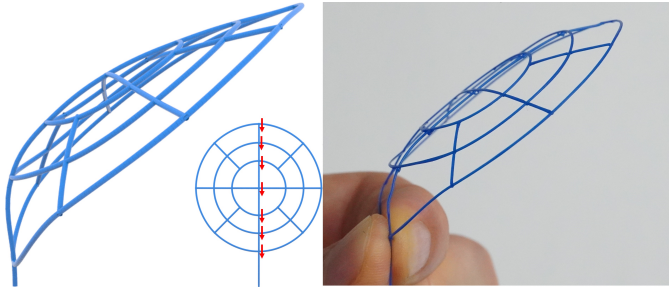


Fig. 9. Actuation example. In this experiment, a single actuation strand is embedded in the structure to induce a planar-to-parabolic deployment upon pulling (red arrow). The simulation result of the actuated structure is shown on the left and the deformation of a physical prototype is shown on the right.

V. CONCLUSIONS

We presented programmable digital weaves—a novel material concept that augments planar elastic grids with sliding connections. Although the experimental results confirm the feasibility of our approach, there are a number of limitations that should be addressed in future work. We do not consider cases where more than two strands cross in one connection. Furthermore, friction between crossing strands is not accurately modeled, which leads to certain amount of discrepancy between our simulation results and the real-world behaviors. We also observed a stiffness bias induced by the extra material required for channels. While beyond the scope of this work, we plan to systematically study the impact of sliding connections on bending stiffness. In particular, sliding connections enable the deployment of a flat patch into a surface with nonzero Gaussian curvature with little resistance, whereas all-fused connections strongly oppose such deformations. Contact beyond EoL nodes and multi-axis response will also be studied in the future. Finally, we would also like to explore the integration of strain sensors using, e.g., Piezo-resist filament [24] to allow for fully-integrated state estimation.

ACKNOWLEDGMENT

We thank Jean Hergel for the initial exploration of the digital weaves, Pengbin Tang and Simon Dünser for the helpful discussions.

REFERENCES

- [1] S. W. Pattinson, M. E. Huber, S. Kim, J. Lee, S. Grunsfeld, R. Roberts, G. Dreifus, C. Meier, L. Liu, N. Hogan, and A. J. Hart, "Additive Manufacturing of Biomechanically Tailored Meshes for Compliant Wearable and Implantable Devices," *Advanced Functional Materials*, vol. 29, no. 32, pp. 1–10, 2019.
- [2] C. Schumacher, S. Marschner, M. Gross, and B. Thomaszewski, "Mechanical characterization of structured sheet materials," *ACM Transactions on Graphics (TOG)*, vol. 37, no. 4, pp. 1–15, 2018.
- [3] K. Bertoldi, V. Vitelli, J. Christensen, and M. van Hecke, "Flexible mechanical metamaterials," *Nature Reviews*, vol. 2, p. 17066, 2017.
- [4] J. Martínez, M. Skouras, C. Schumacher, S. Hornus, S. Lefebvre, and B. Thomaszewski, "Star-shaped metrics for mechanical metamaterial design," *ACM Transactions on Graphics (TOG)*, vol. 38, no. 4, pp. 1–13, 2019.
- [5] T. Djourachkovich, N. Blal, N. Hamila, and A. Gravouil, "Multiscale topology optimization of 3d structures: A micro-architected materials database assisted strategy," *Comput. Struct.*, vol. 255, no. C, Oct. 2021. [Online]. Available: <https://doi.org/10.1016/j.compstruc.2021.106574>
- [6] H. Takahashi and J. Kim, "3d printed fabric: Techniques for design and 3d weaving programmable textiles," in *Proceedings of the 32nd Annual ACM Symposium on User Interface Software and Technology*, ser. UIST '19. New York, NY, USA: Association for Computing Machinery, 2019, p. 43–51. [Online]. Available: <https://doi.org/10.1145/3332165.3347896>
- [7] J. Forman, M. D. Dogan, H. Forsythe, and H. Ishii, "Defextiles: 3d printing quasi-woven fabric via under-extrusion," in *Proceedings of the 33rd Annual ACM Symposium on User Interface Software and Technology*, ser. UIST '20. New York, NY, USA: Association for Computing Machinery, 2020, p. 1222–1233. [Online]. Available: <https://doi.org/10.1145/3379337.3415876>
- [8] M. A. McEvoy and N. Correll, "Materials that couple sensing, actuation, computation, and communication," *Science*, vol. 347, no. 6228, 2015.
- [9] T. L. Buckner, R. A. Bilodeau, S. Y. Kim, and R. Kramer-Bottiglio, "Roboticizing fabric by integrating functional fibers," *Proceedings of the National Academy of Sciences*, vol. 117, no. 41, pp. 25 360–25 369, 2020.
- [10] T. P. Chenal, J. C. Case, J. Paik, and R. K. Kramer, "Variable stiffness fabrics with embedded shape memory materials for wearable applications," in *2014 IEEE/RSJ International Conference on Intelligent Robots and Systems*. IEEE, 2014, pp. 2827–2831.
- [11] T. Hiramitsu, K. Suzumori, H. Nabae, and G. Endo, "Experimental evaluation of textile mechanisms made of artificial muscles," in *2019 2nd IEEE International Conference on Soft Robotics (RoboSoft)*. IEEE, 2019, pp. 1–6.
- [12] J. Shi, S. Liu, L. Zhang, B. Yang, L. Shu, Y. Yang, M. Ren, Y. Wang, J. Chen, W. Chen, Y. Chai, and X. Tao, "Smart Textile-Integrated Microelectronic Systems for Wearable Applications," *Advanced Materials*, vol. 32, no. 5, 2020.
- [13] V. Sanchez, C. J. Walsh, and R. J. Wood, "Textile technology for soft robotic and autonomous garments," *Advanced Functional Materials*, vol. 31, no. 6, p. 2008278, 2021.
- [14] F. Bertails, B. Audoly, M.-P. Cani, B. Querleux, F. Leroy, and J.-L. Lévéque, "Super-helices for predicting the dynamics of natural hair," *ACM Trans. Graph.*, vol. 25, no. 3, p. 1180–1187, Jul. 2006. [Online]. Available: <https://doi.org/10.1145/1141911.1142012>
- [15] M. Bergou, M. Wardetzky, S. Robinson, B. Audoly, and E. Grinspun, "Discrete elastic rods," in *ACM SIGGRAPH 2008 Papers*, ser. SIGGRAPH '08. New York, NY, USA: Association for Computing Machinery, 2008. [Online]. Available: <https://doi.org/10.1145/1399504.1360662>
- [16] M. Bergou, B. Audoly, E. Vouga, M. Wardetzky, and E. Grinspun, "Discrete viscous threads," *ACM Transactions on graphics (TOG)*, vol. 29, no. 4, pp. 1–10, 2010.
- [17] S. Duenser, R. Poranne, B. Thomaszewski, and S. Coros, "Robocut: hot-wire cutting with robot-controlled flexible rods," *ACM Transactions on Graphics (TOG)*, vol. 39, no. 4, pp. 98–1, 2020.
- [18] C. Baek, A. O. Sageman-Furnas, M. K. Jawed, and P. M. Reis, "Form finding in elastic gridshells," *Proceedings of the National Academy of Sciences*, vol. 115, no. 1, pp. 75–80, 2018.
- [19] J. Zehnder, S. Coros, and B. Thomaszewski, "Designing structurally-sound ornamental curve networks," *ACM Transactions on Graphics (TOG)*, vol. 35, no. 4, pp. 1–10, 2016.
- [20] J. Panetta, M. Konaković-Luković, F. Isvoranu, E. Bouleau, and M. Pauly, "X-shells: A new class of deployable beam structures," *ACM Trans. Graph.*, vol. 38, no. 4, Jul. 2019. [Online]. Available: <https://doi.org/10.1145/3306346.3323040>
- [21] G. Cirio, J. Lopez-Moreno, D. Miraut, and M. A. Otaduy, "Yarn-level simulation of woven cloth," *ACM Transactions on Graphics (TOG)*, vol. 33, no. 6, pp. 1–11, 2014.
- [22] G. Sperl, R. Narain, and C. Wojtan, "Homogenized yarn-level cloth," *ACM Trans. Graph.*, vol. 39, no. 4, Jul. 2020. [Online]. Available: <https://doi.org/10.1145/3386569.3392412>
- [23] C. Yuksel, "A class of c 2 interpolating splines," *ACM Transactions on Graphics (TOG)*, vol. 39, no. 5, pp. 1–14, 2020.
- [24] M. Bächer, B. Hepp, F. Pece, P. G. Kry, B. Bickel, B. Thomaszewski, and O. Hilliges, "Defsense: Computational design of customized deformable input devices," in *Proceedings of the 2016 CHI Conference on Human Factors in Computing Systems*, 2016, pp. 3806–3816.